Sascha Grusche,

"Spectral synthesis provides two-dimensional videos on a one-dimensional screen with 360°-visibility and mirror-immunity,"

Appl. Opt. **53**, 674-684 (2014)

Spectral synthesis provides two-dimensional videos on a one-dimensional screen with 360°-visibility and mirror-immunity

Sascha Grusche

Physikdidaktik, Fakultät 2—Pädagogische Hochschule Weingarten, University of Education, Kirchplatz 2, 88250 Weingarten, Germany (saschagrusche@gmail.com)

Received 23 September 2013; revised 5 December 2013; accepted 8 December 2013; posted 0 MONTH 0000 (Doc. ID 198105); published 0 MONTH 0000

Spatial light modulator (SLM)-based tunable sources synthesize any specified spectral power distribution. However, their complexity makes a simpler version desirable. A prism before an SLM-projector is shown to synthesize spectra at least as effectively. Moreover, this simple setup projects two-dimensional (2-D) videos onto a one-dimensional (1-D) screen. Viewed through a prism (or grating), rainbow-colored renderings of grayscale videos emerge. The semitransparent, 2-D virtual images face each viewer all around the 1-D screen. Uncannily, mirrors around the 1-D screen cannot flip the images. In hindsight, SLM-based spectral synthesis is essentially a form of spectral encoding that is applicable to video projection, and beyond. © 2014 Optical Society of America

OCIS codes: (080.0080) Geometric optics; (080.1235) Apparent images; (300.0300) Spectroscopy; (300.6170) Spectra; (330.0330) Vision, color, and visual optics; (330.1730) Colorimetry.

http://dx.doi.org/10.1364/AO.99.099999

1. Introduction

Light sources whose spectrum can be adjusted for specific wavelengths at specific intensities are needed for applications ranging from microscopy and endoscopy [1], colorimetry and color imaging [2–4], to stage lighting [5] and hyperspectral imaging [6–8]. Such tunable light sources are commonly based on light emitting diodes (LED) [9] or spatial light modulators (SLM).

The SLM-based tunable light sources synthesize light usually by subtracting multiple parts from a single spectrum: a white slit image, mostly from a xenon [2,4] or mercury arc lamp, is dispersed by prisms [2,5] or gratings [4,5,10] onto a digital mirror device (DMD) or liquid crystal device (LCD) [2] panel, which masks out parts of the spectrum. Each column of the SLM represents a specific peak wavelength, whose intensity is regulated either by the number of "on" pixels in that column [2,10], or through pulse width modulation [5,11]. Thus, a spectrum is, or rows of spectra are, generated. They are combined into a projected line [11], on a diffusing plate [2], in an integrating cavity [5], in an optical fiber, or in a liquid light guide [4]. For calibration and further use of the light engine, the spectral power distribution (SPD) of the light is measured with a camera [4] or a spectroradiometer [2,12]. An optional feedback loop optimizes the spectral output [2,4,12]. Essentially, such SLM-based light engines are conversions of spectroscopic setups.

This conventional approach to spectral synthesis is intuitive and effective. Conversely, there are two drawbacks. First, a complex apparatus is needed for three major steps: (1) dispersion of white light; (2) SLM-based modification; and (3) recombination. Second, because the SLM is used to encode wavelengths as two-dimensional (2-D) patterns, its potential to encode 2-D images as wavelengths [13] has not been realized with such light engines.

1559-128X/14/010001-01$15.00/0

Correspondingly, I propose an SLM-based light engine that has two advantages. The first advantage is that the setup is simpler, yet at least as effective. It synthesizes light by combining single parts from multiple spectra. This Superposition of Newtonian Spectra (SNS) takes only two steps: (1) SLM-based modification of white light and (2) dispersion. The second advantage is that with the light engine, one can watch 2-D videos from all around a one-dimensional (1-D) projection screen, in a viewing method called Projected-Image Circumlineascopy (PICS).

In Section 2, I introduce the method and setup for SNS spectral synthesis. Based on the synthesized spectra, I compare SNS to other methods of SLM-based spectral synthesis. In Section 3, I translate the essence of SNS into the idea of PICS. I analyze the observed image qualities, and suggest potential applications. Based on PICS, I reinterpret SLM-based spectral synthesis as spectral encoding. In Section 4, I summarize the concepts and findings, and suggest future research.

2. Spectral Synthesis Based on a Superposition of Newtonian Spectra (SNS)

A. Method and Setup

1. *Essence of SNS*

If we disperse a white slit image from a broadband source, we obtain a Newtonian spectrum [14]. Each of its color stripes represents a specific peak wavelength (from λ_B to λ_R). By combining different color stripes from multiple Newtonian spectra, we can synthesize any desired wavelength composition. For this purpose we simply disperse multiple white slit images into multiple Newtonian spectra and superpose the relevant color stripes at a linear locus of spectral synthesis L_S, as in Fig. 1.

2. *SNS Tunable Light Source*

To create multiple white slit images, we projected vertical white lines from an SLM-projector (Epson EB-1750W, mercury arc lamp, 2.600 lumens, LCD, 1280 × 800 pixels, connected to a personal computer or PC). To disperse these horizontally, we used a direct-vision prism as a dispersive element for synthesis (DE_S). A vertical slit in the screen S1 designates L_S (in the y-direction), see Figs. 1 and 2.

Two Newtonian spectra that kiss each other at L_S synthesize light of wavelengths λ_B and λ_R. Intermediate spectra supply intermediate wavelengths to L_S. Thus, the two kissing spectra are our starting point. For these, we disperse two vertical white lines AB and CD (see Fig. 1) whose distance (on S1) equals the dispersive spread [15] (i.e., the distance across which each line is dispersed):

$$\overline{AC} = \overline{BD} = w_S - \Delta x. \quad (1)$$

Here, w_S is the width of each Newtonian spectrum on screen S1, and Δx is the width (in the horizontal x-direction) of each vertical white line on S1.

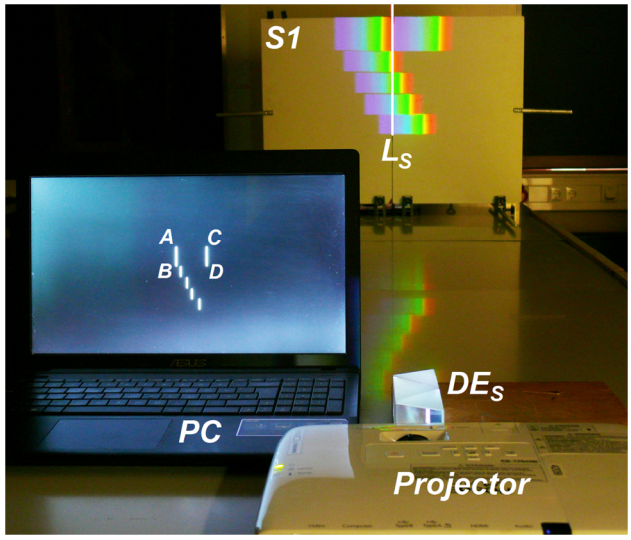

Fig. 1. SNS spectral synthesis. Multiple white lines [as shown on the personal computer (PC) monitor] are projected through a dispersive element for synthesis DE_S, creating multiple Newtonian spectra on screen S1. Each of them supplies a different color stripe (here: red, violet, yellow, green, cyan, and blue) to a slit at the linear locus of spectral synthesis L_S.

Under this kissing condition, the spectra of lines AB and CD barely overlap in a narrow region of width Δx, which we center at the linear locus. There, we synthesize light of wavelengths between λ_B and λ_R by inserting a grayscale pattern of lines between AB and CD.

3. *Analyzing the Synthesized Light*

For qualitative spectral analysis, we place a dispersive element for analysis DE_A (a prism or grating) behind the slit in S1. Thus, we can see the spectrum of the synthesized line of light on a screen S2 behind DE_A. While a prism shows the spectrum only, a transmission grating shows both the synthesized line of light (at diffraction order $m = 0$), and its spectrum (at diffraction orders $m = -1$ and $m = +1$), see Fig. 2. Alternatively, we may view a corresponding virtual image by placing DE_A between our eyes and the line of light on S2.

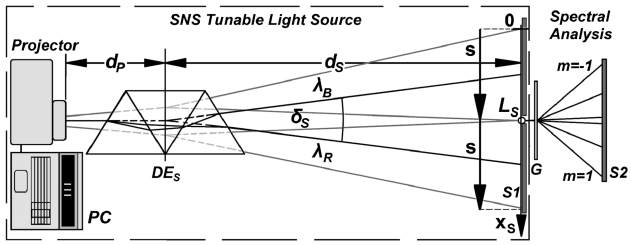

Fig. 2. Setup geometry for SNS (top view). Our setup has $d_P = 0.07$ m; $d_S = 1.93$ m. The light at L_S is let through a slit of width $w = 1 \pm 0.1$ mm and analyzed on screen S2 with a grating G (groove density $g = 1000$/mm). Using coordinates x to describe the undispersed grayscale pattern, we introduce x_S for the dispersed grayscale pattern.

For quantitative spectral analysis, we used a spectroradiometer (JETI specbos 1211) to measure spectral radiance at L_S. The spectroradiometer is connected to the PC. Its measuring software (JETI LiMeS) exports the data into an Excel file.

4. *Calibrating the Grayscale Pattern*

Each horizontal coordinate x in the grayscale pattern on S1 yields a specific peak wavelength $\lambda_{LS}(x)$ at L_S. Hence, the grayscale values $I(x,y)$ of the projected pattern determine the spectral intensity $I_A(\lambda_{LS},y)$ of the synthesized light at L_S.

For wavelength calibration, we measure $\lambda_{LS}(x)$ for 10 equidistant, vertical white lines between AB and CD.

For intensity calibration, we project a uniformly bright rectangle ABCD through DE_S. Varying the overall grayscale value (from 0 to 255), we find that $I_A(\lambda_{LS})$ is roughly proportional to the square of the grayscale value.

Based on this calibration, we compute bitmaps of grayscale patterns for specified spectra. Here, we used a simple heuristic: (1) disperse white rectangle ABCD; (2) measure $I_A(\lambda_{LS})$; (3) at suitable points, estimate by how much $I_A(\lambda_{LS})$ should be decreased (or increased); (4) modulate the grayscale values $I(x)$ with a corresponding weighting function; and (5) repeat steps 2 through 4 until the result is satisfactory.

5. *Setup Geometry and Spectral Bandwidth*

How does the setup geometry affect the spectral bandwidths of synthesized spectral lines? To understand this, consider the geometry of each Newtonian spectrum. With DE_S at a distance d_P from the projector, each white ray is dispersed into different directions for different wavelengths. Suppose the rays for λ_B and λ_R emerge from DE_S under a dispersion angle δ_S, see Fig. 2 (consider δ_S positive if the ray for λ_B can be made to coincide with the ray for λ_R by a clockwise rotation of less than 90° about the vertex). At a distance d_S from DE_S, these two types of rays create two monochromatic images whose mutual displacement, the so-called dispersive displacement for synthesis, is

$$s = 2\,\tan(0.5\delta_S)d_S. \tag{2}$$

If a ray passes a series of dispersive elements, we use Eq. (2) additively.

According to [15], the width of each Newtonian spectrum is

$$w_S = |s| + \Delta x, \tag{3}$$

where Δx is the width of a vertical white line on S1 at a projection distance $D_P = d_P + d_S$.

To indicate the orientation of the spectrum from DE_S, we use a dispersion vector

$$\mathbf{s} = s\hat{\mathbf{x}}_\mathbf{s}, \tag{4}$$

with unit vector $\hat{\mathbf{x}}_\mathbf{s}$ pointing to the right on S1, see Fig. 2, *cf.* Fig. 3.

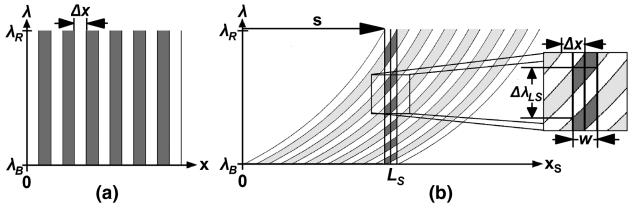

Fig. 3. Deriving spectral bandwidth from dispersion diagrams. 100% spectral intensity is symbolized by white areas, 0% by gray areas. (a) Wavelength distribution of alternating white and black pixels, projected onto screen S1, undispersed. (b) Wavelength distribution of the dispersed pixels (irrelevant parts at lower contrast). We obtained (b) by shearing the wavelength distribution from (a) according to dispersion vector $\mathbf{s}$. Bandwidth $\Delta\lambda_{LS}(x)$ depends on pixel width Δx (on S1) and slit width w.

Applying this geometry to dispersion diagrams [15], we can now translate pixel resolution into spectral resolution (see Fig. 3): a white pixel (projected between x and $x+\Delta x$) yields a certain range of wavelengths at L_S, which we define as the spectral bandwidth $\Delta\lambda_{LS}(x)$. Note in Fig. 3(b) that the curvature of the wavelength distribution mirrors the curve for wavelength calibration $\lambda_{LS} = \lambda_{LS}(x)$. Across Δx, the curve has a roughly constant slope. Thus, if we increase the width of the slit at L_S from $w = 0$ to $w = \Delta x$, the bandwidth doubles. From these two insights, we infer the bandwidth for $w \le \Delta x$:

$$\Delta\lambda_{LS}(x,w) = \left|\lambda_{LS}\left(x - \frac{\Delta x}{2}\right) - \lambda_{LS}\left(x + \frac{\Delta x}{2}\right)\right|\left(1 + \frac{w}{\Delta x}\right). \tag{5}$$

Current video projectors display one white pixel column from the monitor as roughly three grayish pixel columns. This increases Δx proportionally (still, shifting a pixel column by one monitor pixel shifts the line by one projector pixel).

As long as $w \le \Delta x$, shifting a white line by Δx shifts the corresponding spectral line by one full width at half-maximum (FWHM). For any $w \le \Delta x$, the FWHM equals $\Delta\lambda_{LS}$ at $w = 0$, based on Fig. 3(b).

To simplify, we may assume linear dispersion:

$$\lambda_{LS}(x) \approx \lambda_R - \frac{\lambda_R - \lambda_B}{|s|}|x|. \tag{6}$$

Inserting Eq. (6) into Eq. (5), we obtain a spectral bandwidth

$$\Delta\lambda_{LS}(x,w) \approx \left|\frac{\lambda_R - \lambda_B}{N-1}\right|\left(1 + \frac{w}{\Delta x}\right), \tag{7}$$

where $N = w_S/\Delta x$ is the number of projected vertical white lines that would fill ABCD.

B. Results for SNS Spectral Synthesis

On S1, white lines AB and CD had a width $\Delta x = 3 \pm 1$ mm. With $s = 160 \pm 2$ mm, the space between AB and CD took up $10 \pm 0.4\%$ of the width

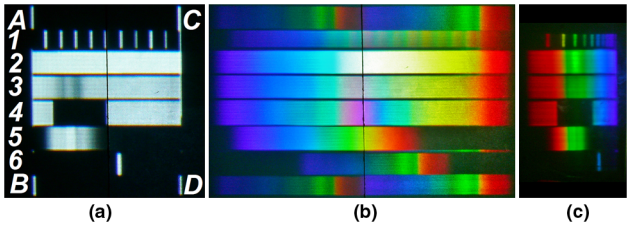

Fig. 4. Photos of SNS spectral synthesis. (a) Projected grayscale patterns on S1. The slit defines L_S. (b) The same patterns, dispersed by DE_S across S1. The Newtonian spectra of AB and CD kiss each other at L_S. (c) The slit spectra on S2 are a rainbow-colored version of the grayscale patterns.

of the black presentation slide. The Newtonian spectra of AB and CD synthesized peak wavelengths $\lambda_R = 667 \pm 1$ nm and $\lambda_B = 435 \pm 1$ nm. Grayscale patterns between AB and CD synthesized geometrically corresponding spectra, see Fig. 4.

A quadratic fit to the peak wavelengths from single white lines (*cf.* Figs. 4 and 5) yielded the wavelength calibration $\lambda_{LS} = 0.0077x^2 - 2.5781x + 666$ (with $[\lambda_{LS}] = 1$ nm and $[x] = 1$ mm). The FWHM of spectral lines ranged from 3 ± 1 nm at λ_B to 8 ± 1 nm at λ_R, see Fig. 5.

The output spectra closely matched the target spectra, see Figs. 6–9. When computing the grayscale patterns, the number of iterations was 39 for the constant SPD in Fig. 6; 40 for the piecewise linear SPD in Fig. 7; 15 for the wide Gaussian SPD in Fig. 8; and 1 for the narrow Gaussian SPD in Fig. 9. For all measurements of spectral radiance, each pattern took up 2.5% of the height of the presentation slide on the monitor, so that it had a height of 2.2 ± 0.1 cm on S1. Only for Fig. 8, the height was casually increased to 33.5 ± 0.1 cm.

C. SNS versus Other Methods of Spectral Synthesis

Superposing single parts from multiple spectra is as effective as subtracting multiple parts from a single spectrum, but less efficient; in SNS, only $w/w_S \leq 1\%$ of the dispersed light was used. An equivalent approach has been used to synthesize infrared spectra, but not visible light [10].

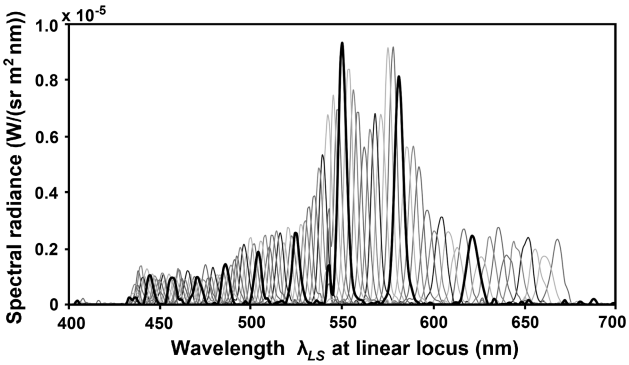

Fig. 5. Spectral lines from every other white pixel column. The heavy, black curve shows the output SPD from pattern 1 in Fig. 4(a).

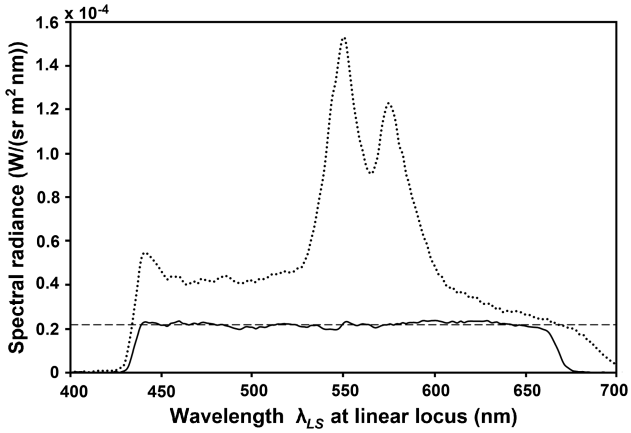

Fig. 6. Illuminant E (dashed). Whereas pattern 2 from Fig. 4(a) yields an irregular SPD (dotted), pattern 3 creates a uniform SPD (solid).

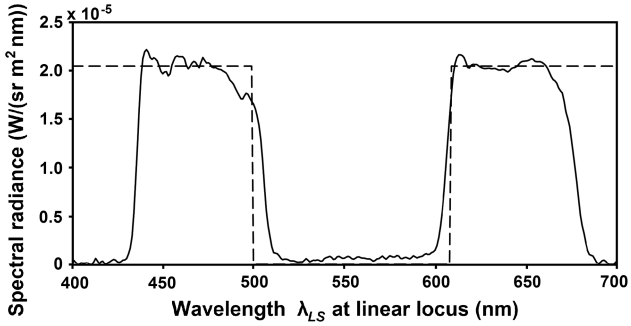

Fig. 7. Magenta. The specified optimum color (dashed) is approximately synthesized (solid) using pattern 4 from Fig. 4(a).

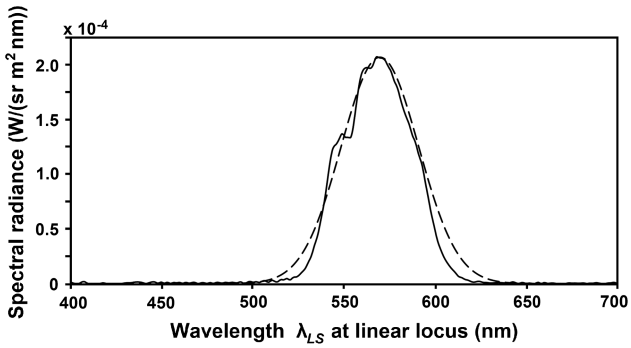

Fig. 8. Gaussian SPD at 570 nm, FWHM = 50 nm. The specified Gaussian (dashed) is approximately synthesized (solid) with pattern 5 from Fig. 4(a).

The SNS setup in Fig. 2 resembles the variable spectrum generator (VSG), but the VSG has a linear variable filter for wavelength selection and a cylindric lens for optical compression [16]. Conveniently, DE_S fulfills both functions.

The spectral accuracy of synthesized SPDs is similar to what is achieved with the spectral integrator [2], although we used a simpler algorithm. Colorimetric purity was even higher with our setup, *cf.* [2]. SLM-projectors with a xenon lamp produce a

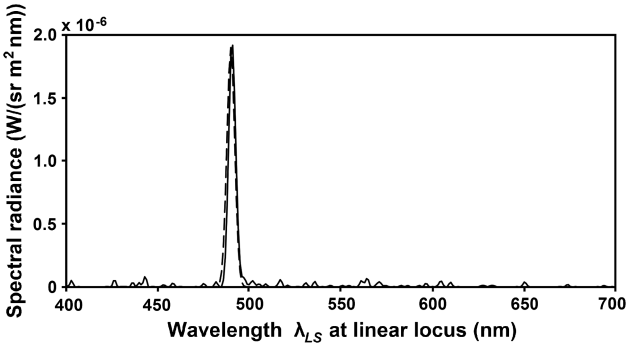

Fig. 9. Gaussian SPD at 490 nm, FWHM = 5 nm. The specified Gaussian (dashed) is closely matched (solid) using pattern 6 from Fig. 4(a).

more uniform spectrum. This should facilitate bitmap computation.

Spectral radiance was higher in Fig. 8 than in Figs. 6, 7, and 9 because we had casually used a taller grayscale pattern. Such overall brightening causes the iris of the projector to dilate. Spectral radiance will further increase if we synthesize 10 lines of light (with one projector), and reflect them into 1 line. Moreover, brighter SLM-projectors (40,000 lumens) are available. If we use the whole presentation slide and optically compress the line of light to a height of 2 cm, the above improvements should raise the uniform SPD in Fig. 8 to about 2 W/(sr m^2 nm). This is one thousand times as bright as what the spectral integrator [2] provides.

Spectral lines from our SNS tunable source are twice as narrow as those from the spectral integrator [2] (our theoretical FWHM based on Eq. (5) with $\Delta x = 4$ mm deviates only ± 1 nm from the experimental FWHM). Based on Eqs. (5) and (7), we can further reduce spectral bandwidth in three ways. First, we may reduce the slit width w. Second, a DE$_S$ with stronger dispersion produces a wider Newtonian spectrum. This lets us increase the distance $|s|$ between AB and CD by a factor of up to nine (*cf.* Fig. 1), thus increasing N (spectral radiance at L_S will not decrease as the wider white rectangle ABCD synthesizes white light, again). Third, increasing the distance d_S between DE$_S$ and L_S increases both $|s|$ and the pixel width Δx.

For SNS, the output SPD is regulated via grayscale values, as with the VSG [16]. In addition, $I_A(\lambda_{LS})$ can be fine-tuned via the number of "on" pixels in a given SLM column, *cf.* [2,10]. This makes our SNS setup a potentially more effective alternative to more complex SLM-based tunable sources.

3. Projected-Image Circumlineascopy (PICS)

A. From the Essence of SNS to PICS Pictures

The SNS tunable source synthesizes a line of light whose slit spectrum is always a rainbow-colored version of the grayscale pattern, see Fig. 4. If we insert grayscale text, photos, or videos between lines AB and CD, DE$_A$ will analyze the line of light into

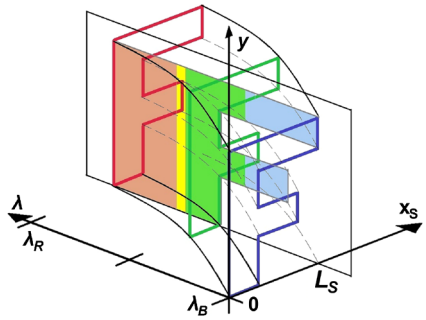

Fig. 10. Imaging principle of PICS. The dispersion diagram shows the wavelength distribution of a white 'F' projected through DE$_S$. As any grayscale image, it consists of congruent, monochromatic images. These are dispersed by DE$_S$ along the x_S-axis, each contributing a different image stripe to the λ-y-plane (at a given coordinate x_S). A dispersive element for analysis DE$_A$ translates the λ-y-plane into two spatial dimensions, thus arranging the image stripes as a rainbow-colored version of the grayscale image.

corresponding rainbow-colored images. To visualize the transformation from grayscale to spectral image, see the dispersion diagram [15] in Fig. 10.

For such spectral images, we used the same setup as for SNS, see Fig. 2. However, for a virtual image that floats in midair, we removed both S1 and S2, placing instead a 1-D projection screen at L_S, see Fig. 11. An opaque 1-D screen (e.g., a metal wire or fine thread) scatters the synthesized light across an azimuthal angle of about 310°. To achieve full 360°-visibility, we need a 1-D screen that is translucent. For this purpose, we used an uncooked capellini (length $l = 26$ cm, diameter $w = 0.9$ mm); it was readily available, extremely cheap, and easy to set up.

The 1-D screen was viewed through DE$_A$, which was at some radial distance d_A from the screen, and some distance d_I from the viewer. The DE$_A$ disperses the synthesized line of light transverse to the line of sight, ensuring that the virtual spectral image faces the viewer directly, see Fig 11. Accordingly, I propose to call this image-viewing method "Projected-Image Circumlineascopy" (PICS), from

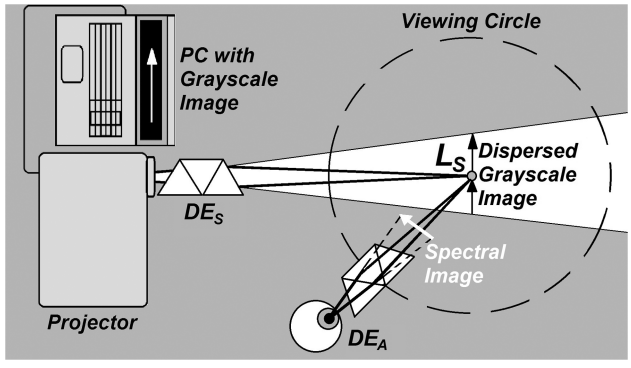

Fig. 11. Use of the SNS tunable source for PICS (top view). A capellini at L_S serves as a 1-D translucent projection screen. It is viewed through DE$_A$, for which we use a direct-vision prism, or a grating ($g = 1000$/mm).

Latin *circum* = "around," *linea* = "a line," and with *-scopy* from the Greek word for "seeing."

B. Results for PICS

1. Overall Appearance

For some views through DE_A, see Figs. 12(b)–12(c) and 13(b)–13(d). The virtual spectral image appeared like a semitransparent banner attached to the capellini. *Viewers walking around the capellini saw the spectral image always turning directly toward them, for 360°*. While the image height looked the same as the height of the line of light on the capellini, the width increased with the distance d_A from DE_A to the capellini. A DE_A with stronger dispersion produced a wider image. Image position, size and sharpness did not notably change for a changed distance d_I between viewer and DE_A.

If the capellini was viewed obliquely from above or below, the image height was foreshortened. If the capellini appeared tilted because of the perspective, the left and right sides of the spectral image were tilted at the same angle. If the capellini was seen from directly above, the spectral image reduced to a line.

To enhance the clarity of the spectral image, the contrast of the grayscale image was increased. If a color image was used instead of a grayscale image, some parts were missing in the spectral image. For example, bright red objects were bright in the red section of the spectral image, but dark in the green or blue section. Still, human faces (and other objects tending toward grayscale) were recognizable in each section.

2. Image Proportions

With a direct-vision prism as DE_A, $d_A = 1$ m was sufficient for viewing. Correct image proportions arose at $d_A \approx 2$ m. With a grating ($g = 1000$/mm) as DE_A, $d_A = 0.5$ m was suitable. At smaller distances, the image became narrow and blurry; at larger distances, the spectral image became wide and faint.

Fig. 12. PICS examples. (a) Original grayscale image of Lena. (b) Spectral image of a capellini. (c) High-resolution spectral image of a capellini.

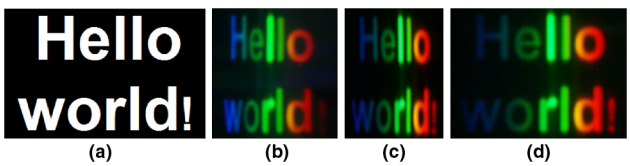

Fig. 13. Different spectral image proportions for different DE_A.

The spectral image had different proportions for different DE_A. This was especially noticeable if text was displayed. Generally, the width-to-height ratio w_A/h_A of the spectral image differed from the width-to-height ratio w_S/h_S of the grayscale image, see Fig. 13 and Section 3.C.2. Specifically, through a direct-vision prism at $d_A = 0.95$ m, the text "Hello world!" of Fig. 13(a) had a $w_A/h_A = 0.5 \pm 0.01\, w_S/h_S$, see Fig. 13(c). Through a series of direct-vision prisms at distances $d_{A1} = 0.95$ m and $d_{A2} = 0.82$ m, the text had a $w_A/h_A = 0.9 \pm 0.02\, w_S/h_S$, see Fig. 13(d). The letters were evenly spaced in both cases. Through the grating at $d_S = 0.4$ m, the text had a $w_A/h_A = 0.6 \pm 0.01\, w_S/h_S$, being squashed toward blue letters, see Fig. 13(b).

3. Image Transformations

Shifting the capellini to the left of L_S (in the negative x_S-direction) removed the right part of the image by shifting the colors. Shifting in the opposite direction effected the opposite.

Shifting the capellini from L_S toward DE_S removed parts from both sides of the image. Shifting the capellini away from DE_S reduced the color range, but left the image intact. In both cases, the image became out of focus, yet it did not notably change within a range of about 0.5 m. Thus, with a series of capellini within that range, a single grayscale image yielded multiple, almost identical, and sharp spectral images at once.

Flipping the dispersive orientation of DE_A caused the spectral image and its colors to flip, as for w_4 in Figs. 16(b) and 16(c). Flipping the dispersive orientation of DE_S caused the spectral image to flip geometrically, but the orientation of the color spectrum remained, *cf.* Fig. 15. Combining both procedures flipped the colors, but not the orientation of the spectral image, *cf.* Figs. 12(b) and 12(c).

In a mirror parallel to the capellini, the spectral image was not flipped, see Fig. 14. Likewise, if a mirror parallel to the capellini reflected the light from DE_S across another parallel capellini, its spectral image had an identical orientation.

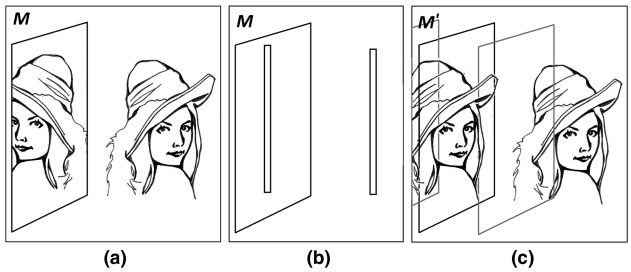

Fig. 14. Mirror-immunity with PICS. (a) A regular 2-D image in front of an upright mirror M is flipped in the mirror; it is not mirror-immune. (b) An upright 1-D screen has an identically oriented mirror image; it is mirror-immune. (c) Hence, even its spectral image (here featuring Lena) is mirror-immune.

4. *Multiple-Screen, Multiple-Image PICS*

With grayscale images beside the original one, as in Fig. 15(a), the spectral images of multiple capellini beside L_S were arranged in space as the capellini themselves. They overlapped for some viewing positions, as in Figs. 15(b)–15(d). The additive color result depended on the spatial sequence in which the capellini were viewed. Some capellini produced a spectrally shifted "doppelgänger" of the spectral image of a neighboring capellini. This happened when the capellini and the projected grayscale images were less than a spectrum width w_S apart, as in Fig. 15.

5. *Image Resolution*

Image resolution was enhanced with L_S further from the projector, whereby the grayscale images could be enlarged in the presentation slide. Additionally, a second direct-vision prism at the projector allowed the grayscale image to take up almost twice as many pixels horizontally. Thus, horizontal image resolution improved, as in Figs. 12(b) and 12(c).

Image resolution depended on the orientation of dispersion because the screen was not perfectly 1-D. To investigate how the width w of the projection screen at L_S affects PICS image resolution, a translucent paper was placed at a distance $d_S = 1.5$ m from the direct-vision prism to scatter the whole dispersed grayscale image. It was viewed through a direct-vision prism as DE_A from behind the paper. Meanwhile, the effective screen width was reduced with a slit aperture directly at the paper (see Fig. 16). Generally, a DE_A with parallel dispersion (relative to DE_S) made the image even blurrier, while an antiparallel DE_A reduced the blurriness. Specifically, if the spectral images were viewed at a distance $d_A = 1.5$ m behind the translucent paper, the difference was extreme. With a parallel DE_A, the spectral image was only sharp for an extremely narrow screen, see Fig. 16(b). With an antiparallel DE_A, the spectral image was sharp for an arbitrarily wide screen, see Fig. 16(c). The same was true for an equivalent setup with gratings. Synthesized on a single blond human hair of length $l \approx 0.5$ m, spectral images appeared equally sharp for both dispersive orientations, yet they were dim.

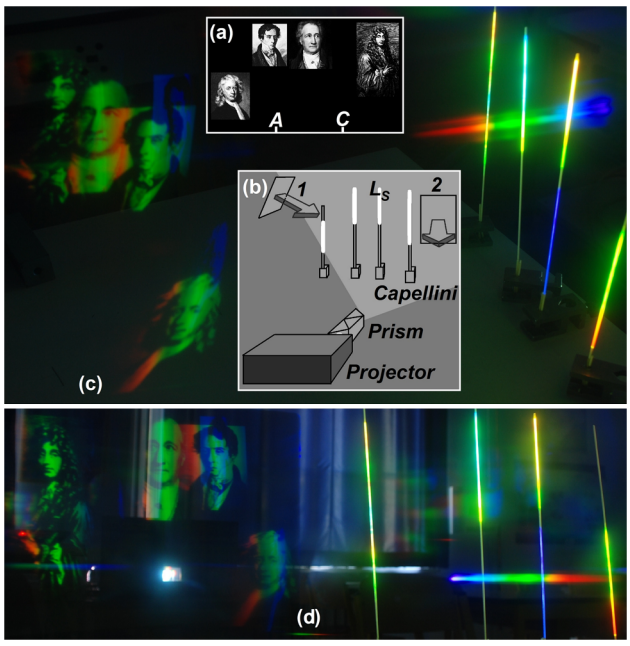

Fig. 15. Multiple-screen, multiple-image PICS. (a) Arrangement of four grayscale portraits (Newton, Fresnel, Goethe, and Huygens) in a presentation slide. (b) The slide was projected across four capellini through a single direct-vision prism as DE_S. Photos (c) and (d) were directly taken through a transmission grating as DE_A at positions 1 and 2. Like rotatable banners attached to the capellini, the spectral portraits always face the viewer. The direct-vision prism at the projector [in photo (d) a white spot] can be flipped horizontally to flip each portrait horizontally.

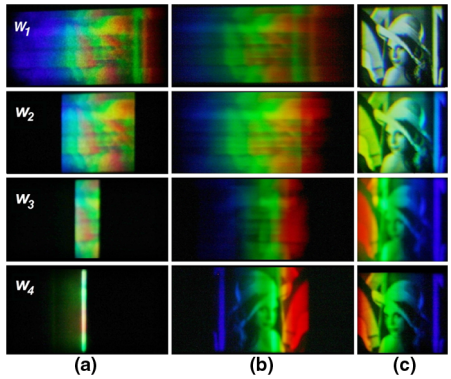

Fig. 16. Image resolution on a 1-D screen, approximated with a 2-D screen. (a) A grayscale image of Lena (looking left) is projected through DE_S so that its constituent monochromatic images are mutually displaced. These yield a blurry image. The 2-D projection screen is successively narrowed (from $w_1 = 17$ cm; $w_2 = 8$ cm; $w_3 = 2$ cm to $w_4 = 0.5$ cm). (b) A parallel DE_A mutually displaces the monochromatic images on the screen even more. Thus, the image gets even blurrier, with Lena still looking left. At $w = w_4$, Lena turns to the right, the image becoming relatively sharp (*cf.* Section 3.C.3). (c) An antiparallel DE_A compensates the displacement among the monochromatic images. These compose a sharp image of Lena looking left.

C. Discussion of PICS Image Properties

1. *Geometry and Colors of the Virtual Spectral Image*

How can we quantify the position, size, orientation, and colors of a virtual spectral image?

Through a direct-vision prism, the spectral image appears centered at the same position as the line of light itself, see Fig. 17. After all, the prism displaces the monochromatic constituents only in the x_A-direction. Through a grating, the spectral image appears to the left and right of the line of light (at $m = -1$ and $m = +1$). The spectral image has the same distance to the grating as the line of light, measured from the point where the central ray (for $\lambda_G = 0.5(\lambda_R + \lambda_B)$) to the viewer passes the grating [17]. In this sense, the spectral image is at the same

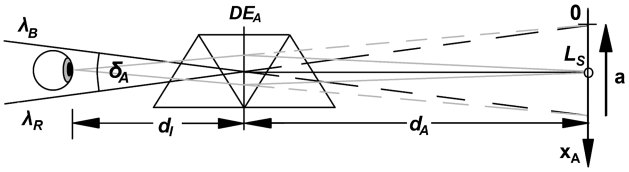

Fig. 17. Virtual image inspected through DE_A (top view) is geometrically analogous to a real image projected through it. (Tracing the dispersed rays to an effective plane of refraction inside the prism simplifies the construction, *cf.* Fig. 2).

distance d_A from DE_A as the line of light, both with the direct-vision prism, and the grating.

As Newton already found in his Experiment XI in Book I, Part II of *Opticks* [18], equal but opposite dispersions by DE_S and DE_A reproduce the original image. This allows us to express, analogous to Eq. (2), the dispersive displacement for analysis for a DE_A with dispersion angle δ_A (see Fig. 17) as

$$a = 2\,\tan(0.5\delta_A)d_A. \tag{8}$$

Analogous to Eq. (3), the width of the spectral image is

$$w_A = |a| + w, \tag{9}$$

w being the width of the 1-D screen, which is assumed to be cylindric, here.

To indicate the orientation of the spectral image seen through DE_A, we use a dispersion vector (analogous to Eq. (4))

$$\mathbf{a} = a\hat{\mathbf{x}}_\mathbf{A}, \tag{10}$$

with the unit vector $\hat{\mathbf{x}}_\mathbf{A}$ pointing to the right of the viewer, see Fig. 17. While **s** determines the coloration of image stripes (*cf.* Fig. 10), **a** dictates the orientation of the spectral image via the order of the color stripes.

Because dispersion in the x_A-direction leaves the view unchanged in the y-direction, the height h_A of the virtual spectral image equals the height h_S of the synthesized line of light, or the height of the projected grayscale image:

$$h_A = h_S. \tag{11}$$

Equations (8)–(11) hold for a prism with negligible magnification, and for a grating. Further, with these equations, we predict the spectral image to have a constant position, size, orientation, and colors even if d_I varies, as long as d_A is constant. Suppose DE_A is not moved relative to the line of light. Then, for a direct-vision prism, d_A is always constant. In contrast, for a grating, the well-known grating formula implies that d_A varies according to the viewer's movements [17]; except along a single moving direction, which is given by the central ray diffracted to the viewer.

The image transformations described in Section 3.B.3 can be understood with Fig. 10 whereby shifting the 1-D screen along the x_S-axis corresponds to shifting the λ–y-plane. Shifting the 1-D screen toward or away from DE_S corresponds to varying the displacement between the monochromatic constituents according to s.

2. *Calculating PICS Image Proportions*

As we saw in the experiment, the spectral image has a different width-to-height ratio than the grayscale image, except at a specified distance d_A, depending on DE_A.

Let us assume the grayscale image extends from line AB to CD, so $w_s/(|s| + \Delta x) = 1$, as in Eq. (3). Then, based on Eqs. (9) and (11), the width-to-height ratio w_A/h_A of the spectral image relates to that w_S/h_S of the grayscale image as follows:

$$\frac{w_A}{h_A} = \left[\frac{|\tan(0.5\delta_A)d_A| + 0.5w}{|\tan(0.5\delta_S)d_S| + 0.5\Delta x}\right]\frac{w_S}{h_S}. \tag{12}$$

Thus, to obtain a spectral image with a specified width-to-height ratio, we may adapt the height of the grayscale image, use different dispersive elements, or change their distances to the projection screen, based on Eq. (12).

To compensate distortions within the spectral image, we adapt the proportions within the grayscale image according to the wavelength scales $x = x(\lambda_{LS})$ of DE_S and $x_A = x_A(\lambda_{LS})$ of DE_A, as Fig. 10 implies.

3. *Calculating PICS Image Resolution*

To grasp PICS image resolution intuitively, remember from Fig. 10 that different image stripes are superposed on the 1-D screen. As an analogy to Fig. 16(a) at $w = w_4$, cut a picture into narrow vertical stripes of width w and stack them. If you then spread the stripes out in the original direction, the original image appears (see Fig. 18(a)), which is analogous to Fig. 16(c) at w_4. If, instead, you spread the stripes out in the opposite direction, a reversed image that is less sharp emerges [see Fig. 18(b)], which is analogous to Fig. 12(b) at w_4.

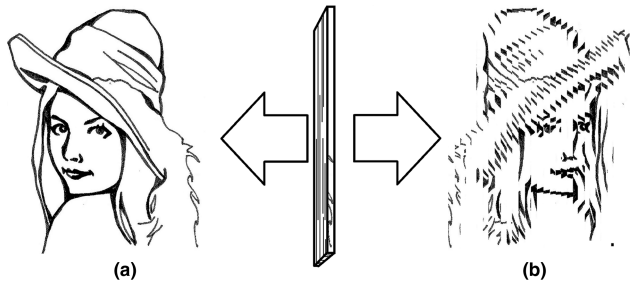

Fig. 18. Analogy for the asymmetry in PICS image resolution: arranging image stripes in reverse order creates a reversed, but blurrier image.

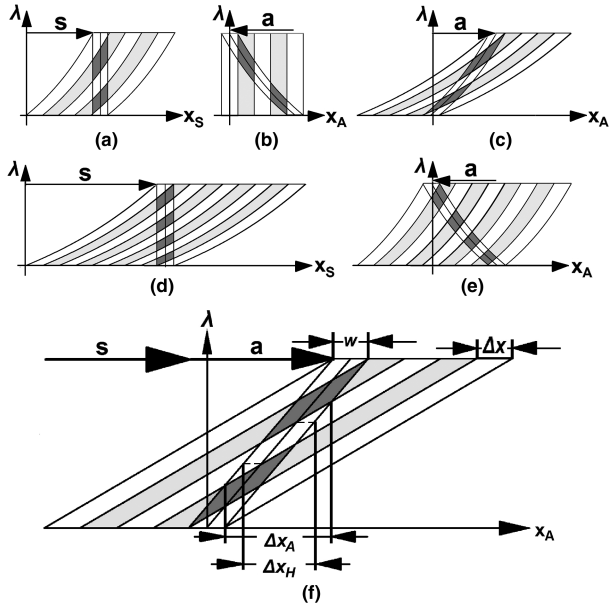

Fig. 19. Deriving PICS spectral image resolution from dispersion diagrams. In (a) and (d), the wavelength distribution of a grayscale image, dispersed by DE_S according to dispersion vector **s**, contains a spectral stack of width w at the linear locus (accentuated) that represents all grayscale pixels as spectral pixels. In (b), (c), and (e), additional dispersion by DE_A shears the spectral stack according to dispersion vector **a**. Thus, the spread-out spectral pixels form a spectral image. Its image resolution depends on the relative dispersive displacement for analysis, a/s. (a) At $a/s = 0$, all spectral pixels are superposed. (b) At $a/s = -1$, all spectral pixels lie next to each other. (c) At $a/s = +1$, spectral pixels partially overlap. In (d), where $a/s = 0$, and in (e), where $a/s = -0.5$, the dispersion of DE_S is twice as strong as in (a)–(c). This allows more pixels to be represented at the linear locus, yielding higher pixel resolution compared to (b). (f) The spectral pixel width Δx_A, and the FWHM of a spectral pixel, Δx_H, depend on the width w of the line of light at the linear locus, on the grayscale pixel width Δx, and the relative dispersive displacement for analysis, a/s.

To describe PICS image resolution quantitatively, we refer to dispersion diagrams [15], see Fig. 19. Let us discuss the straightforward case of direct-vision prisms as DE_A and DE_S. As shown in Figs. 19(a) and 19(d), DE_S shears the wavelength distribution of the grayscale image according to dispersion vector **s**. Thus, at L_S, all grayscale pixels translate into spectral pixels. These are superposed in a spectral stack of width $w \le \Delta x$. Now, consider a viewer who looks in the direction of light projection, so that $\hat{\mathbf{x}}_\mathbf{A}$ is parallel to $\hat{\mathbf{x}}_\mathbf{S}$. Then, DE_A shears the spectral stack, including the spectral pixels, according to dispersion vector **a**.

From Figs. 19(b)–19(c) and 19(e)–19(f), we geometrically derive the pixel width of the spectral image:

$$\Delta x_A = \left|\frac{a}{N-1}\right| + \left|\frac{a+s}{N-1}\right|\left(\frac{w}{\Delta x}\right). \tag{13}$$

With $|s| = (N-1)\Delta x$, we obtain the spectral pixel width

$$\Delta x_A = \left|\frac{a}{s}\right|\Delta x + \left|\frac{a}{s}+1\right| w. \tag{14}$$

Note in Fig. 19 that spectral pixels partly overlap, depending on **a**. Accordingly, we specify a resolution criterion whereby two spectral pixels are just resolved when their distance equals their spatial FWHM, labeled Δx_H. From Fig. 19, we obtain, depending on the relative dispersive displacement for analysis a/s,

$$\Delta x_H = \left|\frac{a}{s}\right|\Delta x, \quad \text{for } \frac{a}{s} \leqq -0.5, \tag{15}$$

and

$$\Delta x_H = \Delta x_A - \left|\frac{a}{s}\right| w, \quad \text{for } \frac{a}{s} \ge -0.5. \tag{16}$$

Finally, let us define the spectral image resolution as the number of spectral pixels that would—based on our resolution criterion—fit within the width of the spectral image, namely as

$$R_A = \frac{w_A}{\Delta x_H}. \tag{17}$$

This is in analogy to the grayscale image resolution, $R_S = w_S/\Delta x$. The asymmetry in the graphs in Fig. 20 depicts our observation that image resolution depends on the dispersive orientations of DE_S and DE_A. Only for vanishing $w/\Delta x$, which means a perfectly 1-D line of light, this asymmetry vanishes.

Now, consider an arbitrary azimuthal viewing direction. Suppose the translucent screen at L_S is flat instead of cylindric, and contains $\hat{\mathbf{x}}_\mathbf{s}$. Then, instead of shearing the spectral stack itself, dispersion vector **a** shears its orthogonal projection onto the x_A axis. Accordingly, we introduce $s_A = \mathbf{s}\hat{\mathbf{x}}_\mathbf{A}$. Generalizing Eq. (13), we get

$$\Delta x_A = \left|\frac{a}{N-1}\right| + \left|\frac{a+s_A}{N-1}\right|\left(\frac{w}{\Delta x}\right). \tag{18}$$

Generalizing Eqs. (15) and (16), we obtain

$$\Delta x_H = \left|\frac{a}{s}\right|\Delta x, \quad \text{for } \frac{a}{s_A} \leqq -0.5, \tag{19}$$

and

$$\Delta x_H = (\Delta x - w)\left|\frac{a}{s}\right| + w\left|\frac{a+s_A}{s}\right|, \quad \text{for } \frac{a}{s_A} \ge -0.5. \tag{20}$$

4. *Suggested Applications of PICS*

The 360°-visibility offers applications from text display to image projection to object tracking [19].

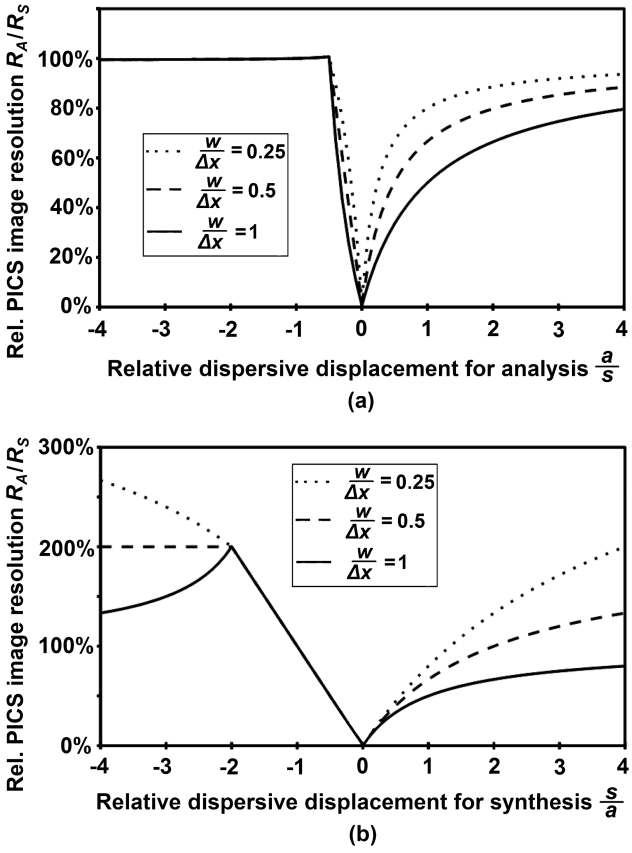

Fig. 20. PICS spectral image resolution in terms of grayscale image resolution, calculated with Eqs. (15)–(17), *cf.* Eqs. (2) and (8). (a) Image resolution is decreased by decreasing the absolute value $|a|$ of the dispersive displacement for analysis, at fixed dispersive displacement for synthesis s. Here, $s = 150\Delta x$. (b) Image resolution is improved by increasing the absolute value $|s|$ of the dispersive displacement for synthesis, at fixed dispersive displacement for analysis a. Here, $a = 150\Delta x$, and R_S refers to the grayscale image resolution at $|s| = 150\Delta x$.

Imagine a cinema where viewers with diffraction glasses sit around a translucent 1-D screen. A grating constant that is proportional to d_A enables correct image proportions. Alternatively, a cylindric transmission grating around the 1-D screen could display correctly proportioned spectral images to anyone around it.

Being semitransparent, virtual images may be superposed onto an object or image, whether for geometric comparison or color experiments. Furthermore, three virtual spectral images of a single 1-D screen may compose a real-color image. To obtain the red, green, blue (RGB) image components, their grayscale versions are inserted in the corresponding intervals (600–700 nm, 500–600 nm, or 400–500 nm, respectively; *cf.* [20]) between AB and CD. However, their superposition requires a specially designed DE_A.

The 1-D screen takes up little space and material. Besides, its light does not disturb a disinterested individual. Moreover, the relevant light beam is narrow, allowing projection in confined or crowded spaces, even for large images. This solves the problem stated in a recently published paper [21].

Being metameric, the synthesized line of light does not betray the image to viewers without or beyond DE_A. This is valuable in police interrogation, medical communication, advertising, and beyond.

Mirror immunity is intrinsic to a 1-D line of light. Spectral images may be multiplied or delivered elsewhere via mirrors parallel to the 1-D screen without ever changing image orientation. They can be duplicated even with a 1-D mirror.

D. Unifying Spectral Synthesis and Spectral Encoding

For PICS, 2-D images are spectrally encoded in 1D. Spectral encoding, whereby locations are translated into wavelengths of light, has already been applied to 2-D image acquisition via 0-D or 1-D apertures, whether in spectrally-encoded endoscopy (SEE) [22], wavelength-multiplexed microscopy [23], or modern pseudoscopy [24]. Spectral encoding has also been proposed for the transmission of a 2-D image via an optical fiber [25–27]. Still, it has not yet been applied to video projection.

Until now, SLM-based light engines were thought to encode wavelengths as patterns on the SLM. Looking back on SNS and PICS, we may now state the reverse: SLM-based light engines encode images as wavelengths. This makes any of these light engines suitable for PICS.

A precursor to both spectral synthesis and spectral encoding is Newton's Experiment I in Book I, Part II of his *Opticks* [18]. Focused on proving his theory, he did not see the practical value of the experiment, however. Nor did Goethe, who repeated the experiment, intent on disproving Newton's theory [28].

4. Conclusion

A dispersed grayscale image contains a line of light whose spectrum is a rainbow-colored version of the image.

This provides (A) a method for synthesizing light with a specified SPD, called SNS; and (B) a method for viewing 2-D images that are spectrally encoded on a 1-D projection screen, called PICS.

For SNS, a prism was placed before an SLM-projector. This setup is at least as effective as other, more complex SLM-based tunable light sources; the trade-off being considerable light loss.

For PICS, grayscale text, photos, and videos from an SLM-projector were horizontally dispersed across an upright capellini. If the capellini was viewed through another prism or grating, rainbow-colored versions of the grayscale images emerged.

Floating in midair, the semitransparent images were correctly oriented for any azimuthal viewing angle. Reflecting the synthesized line of light in a mirror parallel to it did not flip the spectral image. Real-color images are achievable with PICS by superposing three virtual spectral images of a single 1-D screen, yet a three-component viewing device needs to be designed for the RGB mixture.

An advanced version of PICS is conceivable where a 0-D point of light is dispersed into two dimensions, yielding a 2-D spectral image that has correct image proportions and constant apparent size, for any viewing position.

Geometric optics were used in tandem with dispersion diagrams to visualize the transformation from grayscale to spectral image, and to derive formulas for SNS spectral resolution, PICS image proportions, and PICS image resolution.

Future research could investigate PICS image transformations for variations of the setup, for example, with a diagonal 1-D screen. Furthermore, a systematic treatment of generic virtual images in spatial relation to the viewer would be useful.

In retrospect, it has become clear that SLM-based light engines project wavelength-encoded images. These are not limited to abstract patterns, but may as well be concrete images.

I thank Prof. Dr. Florian Theilmann for starting our exploration into spectra in 2010, for commenting on some drafts, and for sending me a direct-vision prism for the experiments. Further, he programmed the algorithm for grayscale bitmaps. However, SPD measurements were only possible because Prof. Dr. Ing. Jörg Baumgart lent me his spectroradiometer, and Dipl.-Phys. Hermann Baumgarten assisted in its use. Finally, I am grateful for the two reviewers' stimulating feedback.

References

1. N. MacKinnon, U. Stange, P. Lane, C. MacAulay, and M. Quatrevalet, "Spectrally programmable light engine for in vitro or in vivo molecular imaging and spectroscopy," Appl. Opt. **44**, 2033–2040 (2005).
2. I. Farup, J. H. Wold, T. Seim, and T. Søndrol, "Generating light with a specified spectral power distribution," Appl. Opt. **46**, 2411–2422 (2007).
3. M.-L. Lo, T.-H. Yang, and C.-C. Lee, "Fabrication of a tunable daylight simulator," Appl. Opt. **50**, C95–C99 (2011).
4. S. Tominaga and T. Horiuchi, "Spectral imaging by synchronizing capture and illumination," J. Opt. Soc. Am. A **29**, 1764–1775 (2012).
5. U. Kanade and M. Joshi, "Programmable light source," U.S. patent 8,107,169 (31 January 2012).
6. J. P. Rice, S. W. Brown, and B. C. Johnson, "Hyperspectral image projectors for radiometric applications," Metrologia **43**, S61 (2006).
7. M. T. Eismann, J. Kerekes, A. P. Schaum, and R. A. Leathers, "Multispectral and hyperspectral imaging: introduction to the feature issue," Appl. Opt. **47**, MHI1 (2008).
8. J. P. Rice, S. W. Brown, D. W. Allen, H. W. Yoon, M. Litorja, and J. C. Hwang, "Hyperspectral image projector applications," Proc. SPIE **8254**, 82540R (2012).
9. I. Fryc, S. W. Brown, G. P. Eppeldauer, and Y. Ohno, "LED-based spectrally tunable source for radiometric, photometric, and colorimetric applications," Opt. Eng. **44**, 111309 (2005).
10. S. W. Brown, J. P. Rice, J. E. Neira, B. C. Johnson, and J. D. Jackson, "Spectrally tunable sources for advanced radiometric applications," J. Res. Natl. Inst. Stand. Technol. **111**, 401–410 (2006).
11. N. R. Nelson, "Hyperspectral scene generator and method of use," U.S. patent 7,106,435 B2 (12 September 2006).
12. T. Horiuchi, H. Kakinuma, and S. Tominaga, "Effective illumination control for an active spectral imaging system," in *Proceedings of the 12th International Symposium on Multispectral Color Science* (Society for Imaging Science and Technology, 2010), pp. 529–534.
13. J. H. Hong, "Wavelength multiplexed two dimensional image transmission through single mode optical fiber," U.S. patent 5,315,423 A (24 May 1994).
14. W. Rueckner, "The Spectrum," http://sciencedemonstrations.fas.harvard.edu/icb/icb.do?keyword=k16940&pageid=icb.page93265.
15. F. Theilmann and S. Grusche, "An RGB approach to prismatic colours," Phys. Educ. **48**, 750 (2013).
16. H. R. Garner, "Variable spectrum generator," U.S. patent 6,657,758 B1 (2 December 2003).
17. M. Müller and L.-M. Schön, "Virtuelle Beugungsbilder am Gitter," in *Didaktik der Physik. Frühjahrstagung Münster*, H. Groetzebach and V. Nordmeier, eds. (PhyDid B, 2011) pp. 1–9, http://phydid.physik.fu-berlin.de/index.php/phydid-b/article/view/288/348.
18. I. Newton, *Opticks: Or, a Treatise of the Reflections, Refractions, Inflections and Colours of Light*, 4th ed. (Dover Publications, 1979).
19. A. Yilmaz, O. Javed, and M. Shah, "Object tracking: a survey," ACM Comput. Surv. **38**, 13 (2006).
20. J.-P. Meyn, "Colour mixing based on daylight," Eur. J. Phys. **29**, 1017–1031 (2008).
21. C.-K. Lee, T. Lee, H. Sung, and S.-W. Min, "Analysis and design of wedge projection display system based on ray retracing method," Appl. Opt. **52**, 3964–3976 (2013).
22. M. Merman, A. Abramov, and D. Yelin, "Theoretical analysis of spectrally encoded endoscopy," Opt. Express **17**, 24045–24059 (2009).
23. A. Schwarz, A. Weiss, D. Fixler, Z. Zalevskya, V. Micó, and J. García, "One-dimensional wavelength multiplexed microscope without objective lens," Opt. Commun. **282**, 2780–2786 (2009).
24. J. Lunazzi and N. Rivera, "Pseudoscopic imaging in a double diffraction process with a slit," Opt. Express **10**, 1368–1373 (2002).
25. D. E. Hulsey and S. K. Case, "Fiber-optic image transmission system with high resolution," Appl. Opt. **22**, 2029–2033 (1983).
26. J. Calatroni, C. Froehly, and T.-C. Yang, "Transmission d'images en couleurs dans des fibres optiques par codage polychromatique," Appl. Opt. **26**, 2202–2205 (1987).
27. D. Mendlovic, J. Garcia, Z. Zalevsky, E. Marom, D. Mas, C. Ferreira, and A. W. Lohmann, "Wavelength-multiplexing system for single-mode image transmission," Appl. Opt. **36**, 8474–8480 (1997).
28. J. W. v. Goethe, *Farbenlehre* (Cotta, 1810). http://www.farben-welten.de/farben-welten/goethes-farbenlehre/enthuellung-der-theorie-newtons/erste-proposition-erstes-theorem-2.html.